

# Structural Characterization of Dendriplexes In Vacuo: A Joint Ion Mobility/Molecular Dynamics Investigation

Fabrice Saintmont, Sébastien Hoyas, Frédéric Rosu, Valérie Gabélica, Patrick Brocorens, and Pascal Gerbaux\*



Cite This: <https://doi.org/10.1021/jasms.2c00122>



Read Online

ACCESS |



Metrics & More



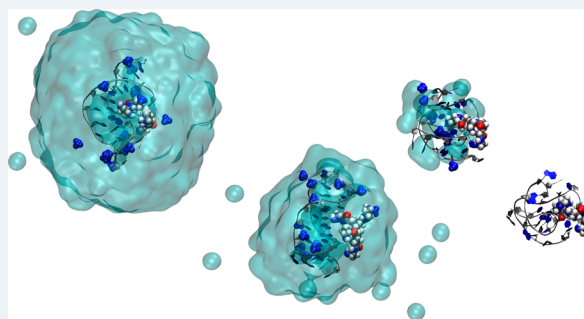
Article Recommendations



Supporting Information

**ABSTRACT:** The combination between ion mobility mass spectrometry and molecular dynamics simulations is demonstrated for the first time to afford valuable information on structural changes undergone by dendriplexes containing ds-DNA and low-generation dendrimers when transferred from the solution to the gas phase. Dendriplex ions presenting 1:1 and 2:1 stoichiometries are identified using mass spectrometry experiments, and the collision cross sections (CCS) of the 1:1 ions are measured using drift time ion mobility experiments. Structural predictions using Molecular Dynamics (MD) simulations showed that gas-phase relevant structures, i.e., with a good match between the experimental and theoretical CCS, are generated when the global electrospray process is simulated, including the solvent molecule evaporation, rather than abruptly transferring the ions from the solution to the gas phase. The progressive migration of ammonium groups (either  $\text{NH}_4^+$  from the buffer or protonated amines of the dendrimer) into the minor and major grooves of DNA all along the evaporation processes is shown to compact the DNA structure by electrostatic and hydrogen-bond interactions. The subsequent proton transfer from the ammonium ( $\text{NH}_4^+$  or protonated amino groups) to the DNA phosphate groups allows creation of protonated phosphate/phosphate hydrogen bonds within the compact structures. MD simulations showed major structural differences between the dendriplexes in solution and in the gas phase, not only due to the loss of the solvent but also due to the proton transfers and the huge difference between the solution and gas-phase charge states.

**KEYWORDS:** dendriplex, DNA, dendrimer, on mobility, molecular dynamics, collision cross section



dendriplexes associating PAMAM G2–4 to a 38-base ss-DNA<sup>16</sup> and PAMAM G3–5 to a 38-base ds-DNA.<sup>18</sup>

Mass spectrometry analysis of intact polyanionic nucleic acids has nowadays acquired sufficient maturity to be considered as a method of choice for the structural investigation of nucleic acids,<sup>19</sup> including nucleic acids complexed to dendrimers.<sup>20</sup> In particular, ion mobility spectrometry (IMS) experiments represent an invaluable analytical method to generate structural data on gas-phase ions.<sup>21</sup> By comparing the measured collision cross sections (CCS) with theoretical CCS obtained on candidate ion structures generated upon MD simulations, description of the gas phase ion structures may be afforded at the molecular level.<sup>21,22</sup> The IMS/MD combination requires that the MD parameters and the IMS calibration are adequately set up, and elegant studies on protein ions,<sup>23</sup> synthetic polymers<sup>24</sup> and dendrimers<sup>25,26</sup> are reported.

## INTRODUCTION

Supramolecular complexes associating nucleic acids (DNA or RNA) and dendrimers are called dendriplexes and are developed for gene therapy with special attention paid to their transfection efficiency and their toxicity.<sup>1</sup> Polyamidoamine (PAMAM) and polypropyleneimine (PPI) dendrimers of different generations bind nucleic acids and improve transfection efficiency, depending on the protonated primary amine/phosphate ratio (N/P), the generation of the dendrimers, the nature of the nucleic acid, and the cell lines.<sup>1–5</sup>

Characterization of dendriplexes relies on gel electrophoresis,<sup>6–9</sup> zeta potential determination,<sup>8,10</sup> atomic force microscopy (AFM),<sup>10,11</sup> dynamic light scattering (DLS),<sup>10,12,13</sup> isothermal titration calorimetry (ITC),<sup>10,12,13</sup> and circular dichroism (CD).<sup>10,12,14,15</sup> Although these analytical methods are efficient to attest to the existence of the supramolecular nucleic acid/dendrimer complexes, they cannot afford a structural description of the dendriplexes at the molecular level. Molecular Dynamics (MD) investigations have recently been introduced for dendriplex structural description.<sup>13,16–18</sup> For instance, Maiti et al. used MD simulations in explicit solvent to investigate the structures of

**Received:** May 4, 2022

**Revised:** July 9, 2022

**Accepted:** July 13, 2022

However, Gabelica et al. demonstrated that gaseous DNA ions are often characterized by more compact structures than in solution, which are not reproduced using MD simulations when the starting point is the fully desolvated canonical double-helix conformation.<sup>27,28</sup> One of the main challenges is the way the phosphate groups are neutralized: in solution, all phosphate groups are deprotonated (and surrounded by a counterion atmosphere<sup>29</sup>), but in the gas phase most of the phosphate groups are neutralized by a proton transfer from the volatile buffer, leaving a number of deprotonated phosphate groups corresponding to the final charge state.<sup>27,28</sup> The protonation of specific phosphate groups adds hydrogen atoms that can form new hydrogen bonds (HB) with other phosphate groups (protonated or not). In 2017, Porrini et al. demonstrated that these HB play a determining role on the compaction of the gas phase ion structure.<sup>28</sup> They studied the compaction of duplex nucleic acids in the gas phase by associating IMS and MD data.<sup>28</sup> Upon IMS experiments on the Dickerson–Drew dodecamer, the most abundant 5<sup>−</sup> ions generated upon electrospray ionization were found to adopt a more compact conformation than the canonical B-form, while higher charge state ions are more extended because of more important Coulombic repulsions.<sup>28</sup> Porrini et al. showed that direct ion formation MD produced extended structures. They then simulated the ion evaporation/desolvation processes starting from a small, charged water droplet containing a negatively charged duplex and ammonium cations.<sup>28</sup> Upon water molecule evaporation, the NH<sub>4</sub><sup>+</sup> cations were observed to interact with the phosphate groups within both the major and minor grooves, resulting in compact ion structures that match the experimental data.<sup>28</sup>

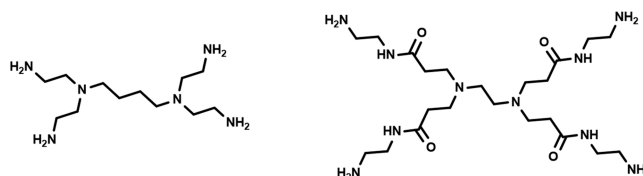
In 2014, Leriche et al. studied for the first time dendriplexes by mass spectrometry methods, including collision-induced dissociation (CID) and ion mobility mass spectrometry experiments.<sup>20</sup> Based on their CID data, the PAMAM/ds-DNA interaction was proposed to be only electrostatically driven, while for a phenyl-modified PAMAM, they suggested that intercalation also contributes to the dendrimer/ds-DNA binding.<sup>20</sup> In that report, even if IMS experiments were conducted, no collision cross sections were provided and no MD simulations were presented to support the experimental-derived conclusions.<sup>20</sup>

In the present study, we intend to investigate by ion mobility experiments and state-of-the-art MD simulations, including the simulation of droplet evaporation, the structures of gaseous ionized dendriplexes, and their DNA component. Two ds-DNA dodecamers with different sequences but identical compositions have been selected. The first sequence, ds-self, is the self-complementary (dCGCGAATTCGCG)<sub>2</sub> Dickerson–Drew dodecamer, whereas the second duplex, ds-HL, is constituted by strands of different masses, AAGGCGGCGGAA and TTCCGCCCTT for, respectively, the “H” (heavy) and the “L” (light) sequences. The dendrimers selected for the study are the PAMAM G0 (E0) and PPI G1 (P1), presented in Scheme 1.

## METHODOLOGY

**Materials.** EDA PAMAM G0 (E0) and the ammonium acetate solution (7 M in water) were obtained from Sigma-Aldrich (Belgium, Overijse). PPI G1 (P1) was obtained from SyMO-Chem B.V. (The Netherlands, Eindhoven). Milli-Q water was obtained with a PURELAB flex from Elga Veolia (Belgium, Anderlecht). The HPLC-grade oligonucleotides were purchased from Eurogentec (Belgium, Seraing). Complemen-

**Scheme 1. Molecular Structures of the Selected Dendrimers: (Left) Generation 1 of Polypropyleneimine (P1) and (Right) Generation 0 of Polyamidoamine (E0)**



tary oligonucleotides at a concentration of  $5 \times 10^{-4}$  M were annealed in Milli-Q water to prepare ds-DNA.

**Collision Cross-Section Notation.** The CCS are abbreviated according to the accepted notation.<sup>30</sup> The notation is in the form <sup>X</sup>CCS<sub>Y</sub>, with X corresponding to the experimental/theoretical method used and Y the drift gas. In our case, the experimental CCS are written down as <sup>DT</sup>CCS<sub>He</sub>, corresponding to a measure using a drift tube (DT) filled with helium as the buffer gas. The theoretical CCS are in the form <sup>TM</sup>CCS<sub>He</sub>, indicating values calculated using the trajectory method (TM) with helium as the collision gas.

**Mass Spectrometry Analysis. Sample Preparation.** Dendrimer/DNA solutions were prepared at a concentration of 5 μM of DNA and 50 μM of dendrimer in Milli-Q H<sub>2</sub>O with 25 mM ammonium acetate. These solutions were used for both the ds-DNA and dendriplex investigations.

**Mass Spectrometry and Ion Mobility Spectrometry Experiments.** MS and IMS experiments were performed on an Agilent 6560 DTIMS-Q-TOF instrument (Agilent Technologies, Santa Clara, CA), with the dual-ESI source operating in the negative ionization mode. A syringe pump flow rate of 190 μL/h was used. Capacitance diaphragm gauges are connected to the funnel vacuum chamber and to the drift tube. An in-house modification to the pumping system allows better equilibration of the pressures: a multiroot vacuum pump ecodyr 40plus (Leybold, Cologne, DE) is connected to the source region with an Edwards SP16K diaphragm valve connected to the front pumping line, while an Edwards E2M80 pump is connected to the Q-TOF region. The helium pressure in the drift tube was  $3.89 \pm 0.01$  Torr, and the pressure in the trapping funnel was  $3.79 \pm 0.01$  Torr. The pressure differential between the drift tube and the trapping funnel ensures that only helium is present in the drift tube. The acquisition software version was B.07.00. All spectra were recorded using soft source conditions.<sup>31</sup> The instrument parameters (electrospray source, trapping region and post-IMS region (Q-TOF region)) were optimized as described elsewhere.<sup>31</sup> The source temperature was set at 220 °C, and the source fragmentor voltage was set to 350 V. The trapping time was 1000 μs, and the release time was 150 μs. The trap entrance grid delta was set to 2 V.

Step-field experiments (five drift tube voltages for each sample) were performed to determine the CCS. The arrival time  $t_A$  is related to  $\Delta V$  (voltage difference between the entrance and the exit of the drift tube region) by

$$t_A = \frac{L^2}{K_0 p_0 T} \left( \frac{1}{\Delta V} \right) + t_0 \quad (1)$$

where  $t_0$  is the time spent outside the drift tube region and before detection. A graph of  $t_A$  vs  $1/\Delta V$  provides  $K_0$  from the slope and  $t_0$  as the intercept. The drift tube length is  $L = 78.1 \pm 0.2$  cm, the temperature is measured accurately by a thermocouple ( $T = 297$

$\pm 1$  K), and the pressure is measured by a capacitance gauge ( $p = 3.89 \pm 0.01$  Torr). The CCS is determined using

$$\text{CCS} = \frac{3ze}{16N_0} \sqrt{\frac{2\pi}{\mu k_B T}} \frac{1}{K_0} \quad (2)$$

The reconstruction of the experimental CCS distributions from the arrival time distributions at the lowest voltage is then performed using equation

$$\text{CCS} = a \frac{z}{\sqrt{\mu}} \times t_A \quad (3)$$

where the factor  $a$  is determined from the  $t_A$  of the peak center at the lowest voltage and the CCS calculated from the regression described above from the peak centers.<sup>32</sup> For broad distributions as reported here, the contribution of  $t_0$  to arrival time broadening is minimal, and this procedure faithfully represents the CCS distribution.<sup>32</sup>

**Molecular Dynamics Simulation. Implicit Solvent Molecular Dynamics.** In solution, assuming that all of the primary amines of the dendrimers are protonated, a net 4+ charge is attributed to the selected dendrimers; see Scheme 1. For the ds-DNA, all of the phosphate groups of DNA are deprotonated in solution, and a global negative charge of 22− is assigned to the selected duplexes. The ds-DNA were built with the Nucleic Acid Builder (nab) module in the standard B-form, and the dendrimers were built based on the Dendrimer Building Toolkit.<sup>33</sup> The parmBSC1 force field was used for DNA<sup>34</sup> and gaff2 for dendrimers.<sup>35</sup> All of the MD simulations were performed with Amber16.<sup>36</sup>

As the dendrimers are smaller than the ds-DNA, the simulated dendriplex structures are likely to depend on the initial relative positions of both partners. To explore a huge number of different assemblies, the input structures for the dendriplexes were created using an original approach that starts by considering a 60 Å radius sphere centered at the center-of-mass of the 22− DNA duplex. By dividing the surface of the sphere in 50 segments and positioning the 4+ dendrimer on a different segment for each input, 50 different starting positions were obtained and numbered from 1 to 50. These input structures were submitted to Molecular Mechanics (MM) simulations counting 10000 steps of steepest descent minimization, followed by a 21 ns MD, both calculations being made in implicit solvent using a generalized Born solvation model<sup>37</sup> with infinite cutoff. Implicit, instead of explicit, solvent was used to decrease the computational time by removing atoms and accelerating the diffusion of the dendrimer toward DNA. The initial ns of the MD corresponded to heating the system from 0 to 300 K, followed by 20 ns at 300 K with a Langevin thermostat and a collision frequency of 1 ps<sup>−1</sup>. The time step was 2 fs with SHAKE constraints for bonds involving hydrogen. We analyzed the last 10 ns of the dynamics to obtain the averaged results. DNA alone was also simulated in solution, applying the same methodology to a unique input structure.

**Protonation of Phosphate/Amine, From Solution to Gas Phase.** As described above, the dendriplexes are formed in solution by associating a positively charged dendrimer and a negatively charged DNA. During the solvent evaporation in IMS experiments, the protons are transferred from the ammonium groups (either protonated dendrimer or NH<sub>4</sub><sup>+</sup> ions) to the vicinal phosphates, leading to a system with a neutral dendrimer and a partially neutralized DNA (five residual negative charges for the most abundant detected ions). This gas-phase proton

distribution was supported by calculating the proton affinities (PA) of NH<sub>3</sub>, of the dendrimer branches, of H<sub>2</sub>PO<sub>4</sub><sup>−</sup> and of deoxycytidine monophosphate (dCMP) using DFT calculations with B3LYP/6-31g(d,p).<sup>38</sup> NH<sub>3</sub> and the PPI and PAMAM branches possess PA at 192, 217, and 234 kcal/mol, respectively, while H<sub>2</sub>PO<sub>4</sub><sup>−</sup> and dCMP have PA at 331 and 316 kcal/mol, respectively. Those results suggest that the proton is preferentially localized on the phosphate groups instead of on the amine nitrogen atoms, pointing to the importance of modeling this proton transfer in our simulations (see below).

**Droplet Evaporation Simulations.** Spherical droplets with an initial radius of 30 Å (2 750 TIP3P water molecules<sup>39</sup>) were built around the dendriplex using packmol.<sup>40</sup> The dendriplex was extracted from the solution MD (see description above); the last geometry of the lowest energy conformer among the 50 starting geometries was selected. Droplets were also built around the DNA alone to evaluate the impact of the presence of the dendrimer. NH<sub>4</sub><sup>+</sup> counterions were added to reach a global charge of 5− (most abundant dendriplex ions in our experiment) by adding 17 NH<sub>4</sub><sup>+</sup> for the ds-DNA and 13 NH<sub>4</sub><sup>+</sup> for the dendriplexes. The energy of the droplets was minimized by MD using 10000 steps of steepest descent with SHAKE constraints for the water model and infinite cutoff. The droplets were then submitted to gas-phase MD at 350 K (about the temperature of the ionization source in the experiments) to progressively evaporate the solvent using a trajectory stitching approach (Langevin thermostat, a collision frequency of 1 ps<sup>−1</sup>, SHAKE constraints for all bonds involving hydrogen, and infinite cutoff).<sup>41</sup>

MD segments of 0.1 ns were run, and after each segment, the water molecules farther than 12 nm from the center of mass of DNA or dendriplex were removed. Two droplet evaporation trajectories were simulated. A first MD was performed, and its final structures were identified by the letter “a”. Analyzing this MD, we found that the duplexes and dendriplexes are still fully solvated after 10 ns. For the second MD, we thus used the droplets of simulation “a” obtained after 10 ns as a starting point and reinitialized the velocities to produce a new trajectory whose final structures are named “b”. This will allow us to evaluate the impact of the droplet evaporation history, resulting in several final structures, for all ds-DNA and dendriplexes.

In addition to the two evaporation trajectories, two proton-transfer protocols were considered in the course of the droplet evaporation simulations:

- (1) The direct proton transfer (DT): the protons from NH<sub>4</sub><sup>+</sup> or the protonated dendrimer are manually (i.e., by the user) transferred to the closest phosphate groups at the end of the evaporation, i.e., after 50 ns, following a procedure described below.
- (2) The progressive proton transfer (PT):
  - For droplets only containing DNA: between 20 and 50 ns, a progressive transfer of protons from NH<sub>4</sub><sup>+</sup> to the closest phosphates was realized. Every 10 segments (every 1 ns), it was checked whether a proton from the NH<sub>4</sub><sup>+</sup> was within 2.5 Å from the oxygen atom of an unprotonated phosphate. If so, it was transferred, leading to a protonated phosphate and NH<sub>3</sub>, that could evaporate as water molecules, i.e., move away from DNA.
  - For dendriplexes: every 1 ns between 15 and 20 ns, it was checked whether the protons on the positively charged terminal amines of the dendrimer were within reach of the phosphates and transferred if so. At 20 ns, if a

terminal amine was still protonated, the proton was transferred to the closest phosphate that can host a proton. Between 20 and 50 ns, the progressive transfer of protons from  $\text{NH}_4^+$  was achieved as described above. The protons were first transferred from the dendrimer, as  $\text{NH}_4^+$  are smaller and can move more freely to interact with the remaining negatively charged phosphates. This distinction between dendrimer protonated amines and ammonium was performed to facilitate the simulations and not to represent what happens in the ESI mechanism.

Previous simulation studies began addressing proton mobility in ESI experiments. Mobile proton simulations were performed for gas-phase simulation of protein based on the proton affinities of the amino acids that can donate or accept protons without the desolvation process.<sup>42–44</sup> Konermann et al. modeled the proton hopping from  $\text{H}_3\text{O}^+$  to neighboring water molecules in a water droplet evaporation simulation, for example, in the absence of analyte molecules.<sup>45</sup> To the best of our knowledge, the transfer of protons to the analyte molecule during droplet evaporation simulation has never been reported.

After 50 ns, the temperature was increased to 375 K and the duration of the segments used to check whether the water molecules can be removed was increased to 1 ns until only 10 molecules of water and the  $\text{NH}_4^+$  ions (and also  $\text{NH}_3$  for PT) remained. Then the protons of  $\text{NH}_4^+$  (and of the dendrimer for DT) were transferred to the closest phosphates, and the water and  $\text{NH}_3$  molecules were removed manually. The force field parameters used for the protonated phosphate were provided by Orozco.<sup>28</sup> The last 10 molecules of water were manually removed as they are the longest to evaporate. Their evaporation could take several tens of nanoseconds at the current temperature. It is common practice to increase the temperature to 450 K to force the evaporation.<sup>28,41</sup> However, the structure of the complex will be more artificially modified by a temperature increase than by manual removal of the few remaining molecules. The water evaporation was usually quicker with the progressive proton-transfer protocol compared to the direct transfer at the end, probably due to the decrease in the number of point charges. At the end of the evaporation and proton transfer, the structures were submitted to gas-phase MD as described below.

**Gas-Phase MD Simulations.** Besides the structures obtained by droplet evaporation, gaseous protonated structures were directly built by arbitrarily positioning the protons all along the DNA backbones, in the so-called local charge model (LC). This protonation method is computationally effective, as there is no calculation, but the work of Porrini et al. showed that simulating the evaporation process influences the structure adopted in gas phase.<sup>28</sup>

To build LC models of 5– duplex or dendriplex ions, we estimated (based on the DFT calculations) that the dendrimer is best described as fully neutralized, whereas only five phosphate groups remain unprotonated on DNA. The negative phosphate groups were arbitrarily positioned to maximize the distance between them, based on the canonical B-form. As there are five charges for two strands, one bears three charges and the other bears two, leading to two possibilities that were both simulated and named “A” and “B”. The structures obtained by solution-phase MD were used to create the input. For DNA, the last structure was selected, while for dendriplexes, among the 50 simulations, the five most stable final structures were used.

Regardless the origin of the inputs, i.e., LC or droplet evaporation, the structures were minimized by 10000 steps of steepest descent before performing 500 ns of gas phase MD at 300 K with a Langevin thermostat, a collision frequency of  $1 \text{ ps}^{-1}$ , and an infinite cutoff. All of the analyses were carried out on the last 200 ns of the dynamics.

**HB Heat Map.** The HB heat maps were built using the “hbond” module in cpptraj<sup>46</sup> to count the number of HB between a residue of one strand and all the residues of the second strand, for DNA in DNA duplexes and dendriplexes, and also HB between dendrimer residues and all DNA residues for dendriplexes, averaged over the analyzed dynamics. Two different heat maps were constructed; one with all HB and a second with only the Watson–Crick (WC) HB counted and averaged depending on the base pair (3 HB for CG and 2 HB for AT). The criteria used to count the HB were set to default, i.e., a  $135^\circ$  angle and 3 Å for the donor–acceptor distance.

**CCS Calculations.** The  $^{\text{TM}}\text{CCS}_{\text{He}}$  calculation was achieved by using 200 frames on the last 200 ns of the gas phase dynamics for DNA and dendriplexes, with both LC and droplet evaporation models, using Collidoscope.<sup>47</sup>  $^{\text{TM}}\text{CCS}_{\text{He}}$  are then averaged values over the 200 frames with the standard deviation as the uncertainty.

## RESULTS AND DISCUSSION

### Electrospray Ionization of the Dendriplex Solutions.

Dendriplexes were analyzed in the negative ionization mode. The infused solutions (25 mM ammonium acetate) contained a 10-fold excess of dendrimers relative to ds-DNA to increase the production of 1:1 complexes and to explore putative higher stoichiometries. Note that the ammonium acetate concentration was lower than commonly used for ds-DNA analysis<sup>28</sup> to avoid the competition between protonated dendrimers and  $\text{NH}_4^+$  cations for the ds-DNA complexation.

In the ESI(–) mass spectra presented in Figure 1, ds-DNA ions and dendriplex ions with [1:1] and [2:1] stoichiometries—

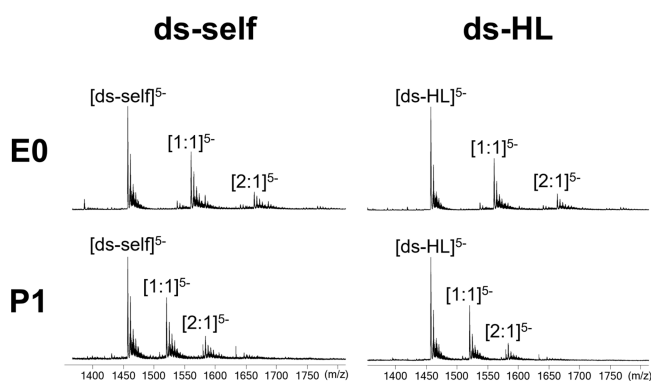


**Figure 1.** ESI(–) analysis of four dendriplex solutions (Agilent 6560 DTIMS-Q-TOF/25 mM ammonium acetate) combining two ds-DNA (5  $\mu\text{M}$ ), i.e., ds-self and ds-HL, with two dendrimers (50  $\mu\text{M}$ ), i.e., E0 and P1. [x:y] represents the stoichiometry of the dendriplex ions with x and y corresponding to the dendrimer and the duplex, respectively.

one and two dendrimers for one ds-DNA, respectively—were detected as 5– ions, raising the question of the charge distributions between the dendrimer and the ds-DNA moieties within the gaseous dendriplex ions. In the upcoming paragraphs, we will describe the combination between ion mobility experiments and molecular dynamics simulations to establish the molecular structures of the [1:1] dendriplex 5– ions, based

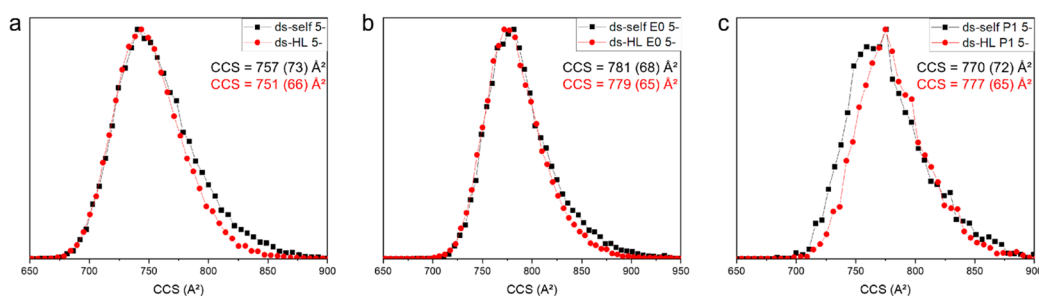


**Figure 2.** DTIMS analysis of ds-DNA and dendriplexes on an Agilent 6560 DTIMS-Q-TOF spectrometer: CCS distributions of (a) ds-self 5<sup>−</sup> (black square) and ds-HL 5<sup>−</sup> (red circle) and of [1:1] dendriplex 5<sup>−</sup> ions containing (b) E0 and (c) P1 dendrimers. The CCS values of the apex are noted on the graphs, with the FWHM in brackets, and are obtained by fitting the distributions with gaussians.

on the comparison between experimental and theoretical collision cross sections. The conformations of dendriplex ions will further be compared to those of the ds-DNA 5<sup>−</sup> ions to monitor the impact of the dendrimer complexation on the nucleic acid structure.

Figure 2 presents the <sup>DT</sup>CCS<sub>He</sub> distributions of ds-DNA 5<sup>−</sup> ions, namely ds-self and ds-HL, and of the [1:1] dendriplex 5<sup>−</sup> ions (ds-self/ds-HL and E0/P1).

The CCS distributions of the ds-DNA 5<sup>−</sup> ions are nearly superimposable, with maxima at 750 Å<sup>2</sup> in nice agreement with recent literature data. For instance, the values for ds-DNA 5<sup>−</sup> ions are close to the value of 735 Å<sup>2</sup> obtained by Porrini et al. for the Dickerson–Drew dodecamer (ds-self).<sup>28</sup> The CCS distributions of the dendriplex 5<sup>−</sup> ions are slightly shifted toward larger values, by about 20 Å<sup>2</sup>, due to the additional presence of the dendrimer. Again, nearly superimposable CCS distributions are recorded for the dendriplex ions, as shown in Figure 2, even if the nature of the dendrimer slightly impacts the CCS of the dendriplex ions, with P1 giving smaller CCS than E0. This is consistent with the dendrimer ion CCS determined in a previous study, i.e., 117 and 155 Å<sup>2</sup> for P1 and E0 with a 1+ net charge, respectively.<sup>25</sup> The 6 CCS distributions are also characterized by a high CCS FWHM (Full Width at Half Maximum) around 65–70 Å<sup>2</sup>, probably indicating different ion conformations with close CCS. Indeed, for more conformationally restricted nucleic acid ions, such as G-quadruplexes, the FWHM in similar ion mobility experimental conditions are most of the time much lower, 20 Å<sup>2</sup>.<sup>32</sup> The FWHM values being very similar between ds-DNA and dendriplex ions, we believe that the complexation of ds-DNA by dendrimer neither reduces nor increases the conformational freedom.

**Molecular Dynamics Simulations. Implicit Solvent MD.** The dendriplex formation occurred within the first 5 ns of the implicit solvent MD simulation. When the dendriplex ions (18<sup>−</sup>) are formed, the dendrimers remain at the initial interaction site on the MD time scale (21 ns). Only the five most stable structures were further considered, and the relative energies are gathered in Table S1. The data set shows that the energy standard deviation over the last 10 ns of the MD simulation is around 21 kcal/mol, which is larger than the energy difference between the first and the fifth most stable structures. The structures of the dendriplexes are presented in annexes (Figures S1,3,5,7), showing a great structural diversity within a small relative energy range. Typical examples are presented in Figure 3 and correspond to two stable dendriplex ion structures associating ds-HL with P1 but presenting significantly different level of compaction. The dendrimer counterpart is located in the minor or the major groove for most of the structures, but no

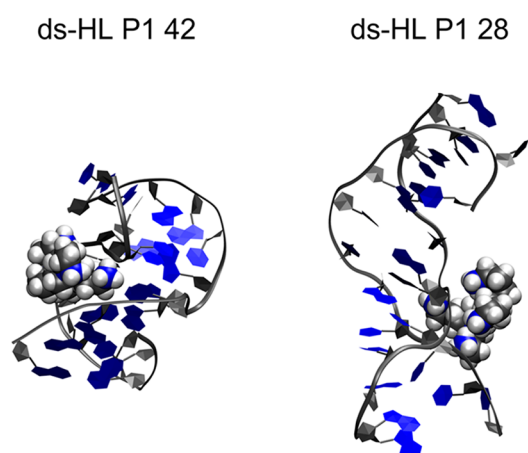


**Figure 3.** Last frames of the implicit solvent MD for dendriplexes (18<sup>−</sup>) formed between ds-HL (22<sup>−</sup>) and P1 (4+). The DNA backbone is in gray and the nucleobases in blue. The dendrimer atoms are represented as vdW spheres with colors representing the nature of the atoms: carbon (gray), hydrogen (white), and nitrogen (blue). The numbers (28 vs 42) correspond to the input numbers.

specific site or sequence specific interactions, i.e., interactions dependent on the nucleotide sequence, were detected. The small energy differences between these simulated conformations suggest that several conformations should exist in solution.

The interactions between dendrimers and ds-DNA and their influence on the conformations are worth investigating. As a visualizing tool, HB heat maps were built and are presented in Figures S2,4,6,8. In these heat maps, each axis represents one DNA strand numbered from 1 to 12, with the numbers corresponding to the residues (nucleotides) (Figure 4). For the dendriplexes, the two axes are prolonged by numbers from 13 to 17 for the dendrimer H-bond donors/acceptors: 13 and 14–17 corresponding to the dendrimer core (up to the carbonyl groups for PAMAM) and to the dendrimer branches (NH-CH<sub>2</sub>-CH<sub>2</sub>-NH<sub>3</sub><sup>+</sup> for PAMAM and CH<sub>2</sub>-NH<sub>3</sub><sup>+</sup> for PPI), respectively (Figure 4). The formation of HB between residues is represented by a colored square, whose intensity accounts for the recurrence of the specific HB all along the MD simulations (Figure 5), since the HB are averaged over the entire MD. For each system, two heat maps are built. First, the global HB heat map, i.e., presenting all the HB present in the ion structure, contains the contribution of all DNA/DNA HB interactions (for DNA modeled with or without the dendrimer) and of dendrimer/DNA HB (for dendriplexes). The second HB heat

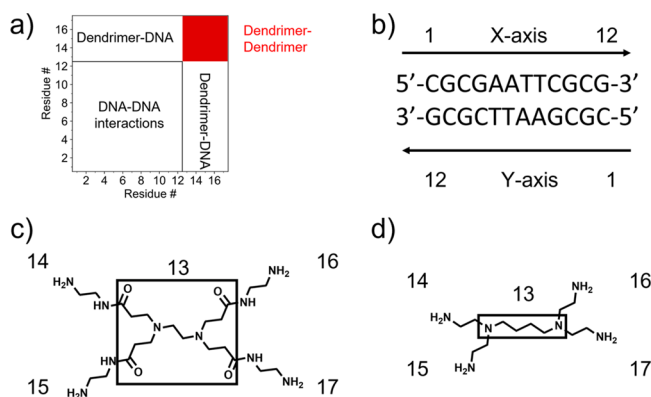


**Figure 4.** Representation of a global HB heat map (a) highlighting the position of the different HB interactions. The residue numbering for DNA (b), PAMAM G0 (c), and PPI P1 (d) is presented.

map specifically focuses on the Watson–Crick (WC) HB with normalization of the number of HB by 2 or 3, depending on the AT or CG interaction, respectively. For the global HB heat maps of dendriplexes, the sections corresponding to DNA/DNA and dendrimer/DNA interactions are separated, as shown in Figure 4, to visualize the HB partners. For HB between DNA and dendrimer residues, all possible HB are counted without discrimination between base and phosphate HB.

By first considering the ds-DNA 22<sup>-</sup> ions, we observed similar HB distributions whatever the sequence. In the HB heat maps in Figure 5, a diagonal is present and corresponds to the WC base pairing characteristic of the B-form. For all global heat maps (Figure 5a,c), four light gray squares are observed among black squares and are readily attributed to the AT base pairs, as they contain only two HB instead of three for the GC base pairs. The WC heat maps (Figures 5b and d) represent only the WC HB, and those bonds have been normalized, meaning that the AT and GC base pairs should appear with squares of same intensity provided they have the same persistence. However, weak color differences are still detected for AT base pairings, especially when they are located at the extremities of the helix, and highlight that the AT base pairings, weaker than the GC ones, are suffering intermittent dissociations during the MD simulations.

The MD simulations of dendriplexes (18<sup>-</sup>) in implicit solvent reveal that the WC HB base pairings are essentially preserved, with only weak perturbations of the HB pattern in the AT regions for both ds-self and ds-HL dendriplexes (Figure 6). However, whereas ds-HL E0 39 that presents weak deformations of the helix has lost the WC HB at the extremities, the

highly deformed structure of ds-HL P1 42 conserves the full WC base pairing diagonal (Figure 6).

The dendriplex HB maps are efficient to establish the interaction site between the ds-DNA and the dendrimer, i.e., the position of the dendrimer on the nucleic acid helix, as exemplified in Figure 7. Indeed, in the DNA/DNA interaction boxes, the top-right region corresponds to the minor groove, and the bottom-left region to the major groove. By projecting both ss-DNA/dendrimer HB interactions in the DNA/DNA box, the crossing area highlights the dendrimer/ds-DNA interaction, either in the major or the minor groove, as represented in Figure 7 for four selected dendriplexes.

**Gas-Phase Molecular Dynamics Simulations.** The ds-DNA ions (22<sup>-</sup>) and dendriplex ions (18<sup>-</sup>) generated in solution must be partially neutralized to reach the 5<sup>-</sup> charge state of the experimentally detected gas phase ions (Figure 1). Seventeen and thirteen protons must thus be added to the ds-DNA and dendriplex species, respectively, raising the question of their positions along the ds-DNA backbone and/or on the dendrimer primary amines.

**Molecular Dynamics Simulations on Gaseous ds-DNA 5<sup>-</sup> Ions.** The easiest way to create an isolated ion from a DNA duplex is to randomly neutralize the phosphate groups, considered as fully deprotonated in solution at pH 7 (25 mM CH<sub>3</sub>COONH<sub>4</sub>), until reaching the targeted charge state (5<sup>-</sup> here). Using this procedure, named Local Charge Model (LC model), many protomers can be prepared when arbitrarily neutralizing phosphate groups. In the present study, the protons were added to maximize the distance between the residual negative charges and, considering the odd charge state (5<sup>-</sup>), two structures, named A and B in this section, were created due to the nonsymmetric charge distribution between both strands (see methodology for more details). These input structures were then submitted to MD simulations in vacuo to generate candidate structures whose theoretical CCS (<sup>TM</sup>CCS<sub>He</sub>) are calculated using the Trajectory Method implemented in Collidoscope.<sup>47</sup> Table S2 compares the experimental (<sup>DT</sup>CCS<sub>He</sub>) and theoretical (<sup>TM</sup>CCS<sub>He</sub>) CCS for both the ds-DNA 5<sup>-</sup> ions detected in Figure 1. As discussed in the recent literature,<sup>28</sup> unbiased MD on gaseous nucleic acid ions systematically generates extended structures because of the preponderance of the repulsive electrostatic contribution. In this work, the theoretical CCS are between 18 and 35% (see Table S2) higher than the experimental ones, clearly pointing to the generation during MD of extended structures that are not relevant to the experimental structures. This is clearly observed in Figure S9 that shows extended duplex structures with highly distorted helices. The protonated phosphate groups are involved

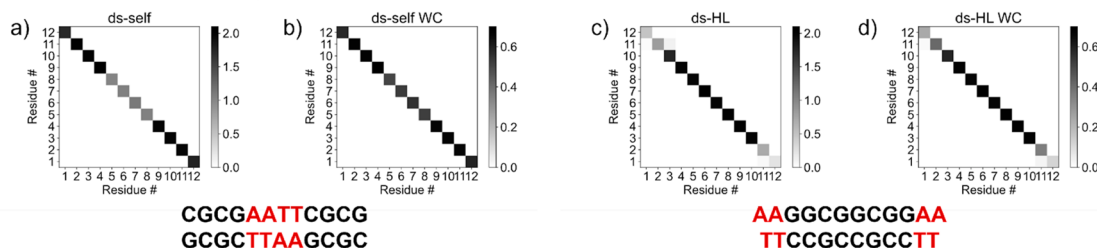


**Figure 5.** HB analysis of ds-DNA (22<sup>-</sup>) simulated in implicit solvent by Molecular Dynamics: heat map representation of HB between the residues of the two strands (one strand at the X axis and the other at the Y axis, each numbered from 1 to 12). For each ds-DNA, i.e., ds-self and ds-HL, two different HB heat maps are built: (i) a global HB heat map (a and c) presenting all the HB present in the structure and (ii) a WC HB heat map that only presents the WC HB, after normalization (b and d).

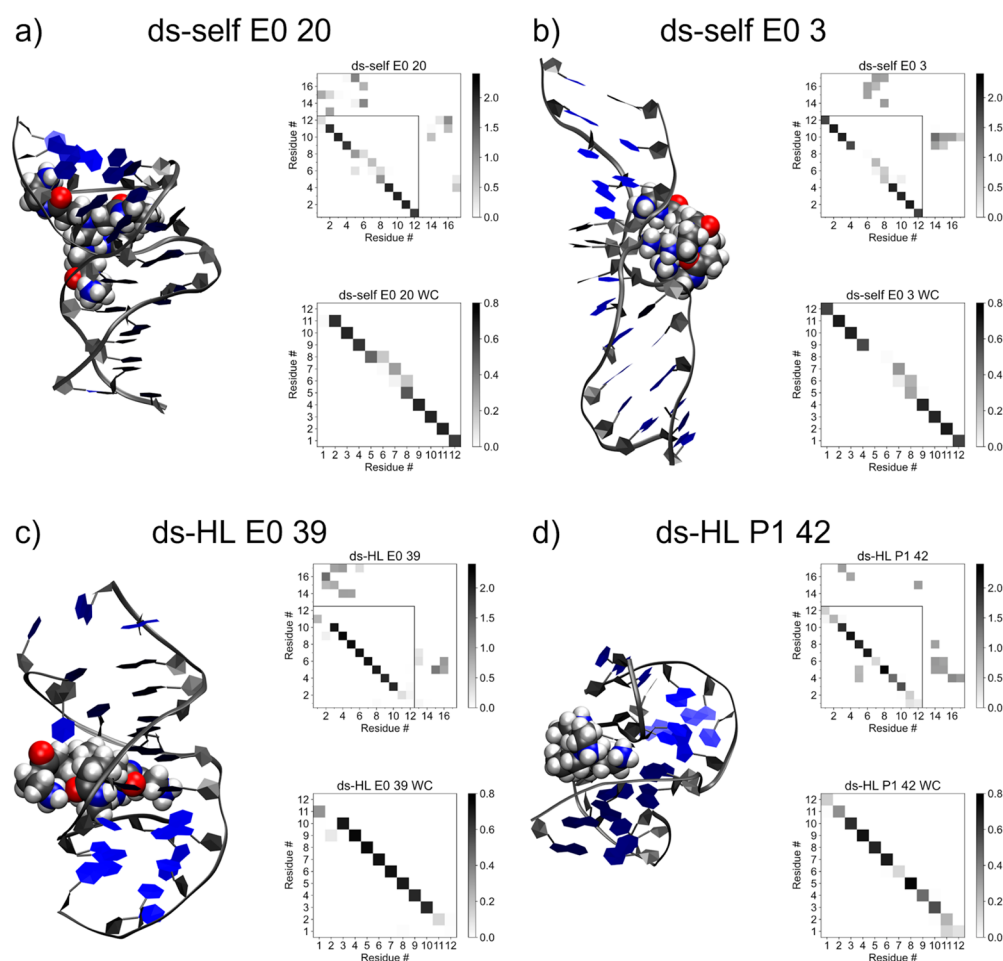


**Figure 6.** Selected snapshots of the last frames of the MD in implicit solvent for selected dendriplexes, associating (a) ds-self and E0, (b) ds-self and E0; note that structures (a) and (b) are generated from different dendrimer/DNA starting points, (c) ds-HL and E0 and (d) ds-HL and P1. The HB heat maps present the HB interactions between the residues of each strand and with those of the dendrimer. For each structure, two different HB heat maps are built: (i) a global HB heat map (top) presenting all the HB present in the structure and (ii) a WC HB heat map (bottom) that only presents the WC HB and after normalization.

in HB between the strands, as exemplified in Figure S10, and the HB network between the complementary bases is disturbed as highlighted by the HB heat maps presented in Figure S11. Briefly, for these extended ds-DNA structures, the WC base pairing is partly conserved from the solution to the extended gaseous structures, especially for the GC base pairs, and additional HB are detected between the phosphate groups in the minor groove, as already described by Porrini et al.,<sup>28</sup> stabilizing the extended gas phase ion conformations.

Porrini et al. showed that the ds-DNA ion structures that are most representative of the experimental data can be obtained by simulating the desolvation process occurring in the electrospray source, i.e., producing the gaseous ions from the solution.<sup>28</sup> A 30 Å water droplet was thus created, containing ds-DNA (structure obtained in implicit solvent simulations as starting structure, 22−), 2750 water molecules, and 17 NH<sub>4</sub><sup>+</sup> cations to reach a global charge of 5− (see Methodology). The droplet was subjected to gas-phase MD at 350 K to progressively evaporate the water molecules. While water was evaporating, the evaporation slowed down (see Figure S12), and the temperature was thus increased to 375 K to accelerate the process. Upon ESI, naked ds-DNA 5− ions are produced upon proton transfer from the ammonium ions to the phosphate groups, producing ammonia as a volatile byproduct.<sup>28</sup> Because such a transfer is

not accessible using our MD tools, the neutralization of the phosphate groups must be manually performed, following two protocols: (i) at the end of the simulation, when almost all water molecules have been evaporated or (ii) sequentially all along the MD simulations. These two protocols are named direct proton transfer (DT) and progressive proton transfer (PT) in the next discussions.

Snapshots of the evaporation process for ds-DNA (Figures S13–16) show that a fully solvated DNA double helix only presents weak deformation after 20 ns for ds-self, whereas significant deformation is already detected after 3.5 ns for ds-HL, with the zipping of the major groove by the ammonium cations, i.e., the strands getting closer in the groove as shown in Figure 8A. After 50 ns, the droplets are almost fully evaporated, and the duplex ions are no longer solvated. All structures are highly modified, and modifications persist during the last part of the evaporation, when the temperature is increased (see Figure 8B). When using the progressive proton transfer protocol (PT) instead of the direct proton transfer protocol (DT), more extended structures are obtained, as shown in Figure 8C for example.

After their complete desolvation/partial neutralization, the 5− ds-DNA ions were submitted to gas phase MD, their <sup>TM</sup>CCS<sub>He</sub> were calculated over the last 200 ns and compared to

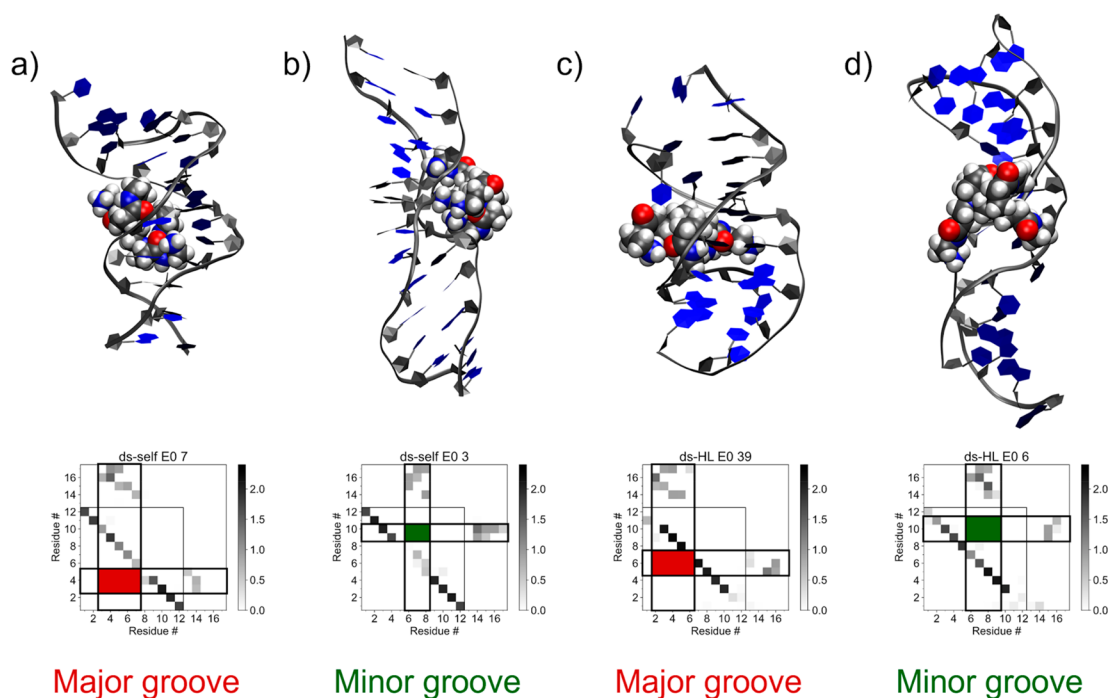


**Figure 7.** Last frames of the implicit solvent MD for dendriplexes between E0 dendrimer and (a, b) ds-self for inputs 7 and 3 and (c, d) ds-HL for inputs 39 and 6. The corresponding heat maps for all HB are represented on the bottom and show a crossing area indicating the interaction site between DNA and dendrimer.

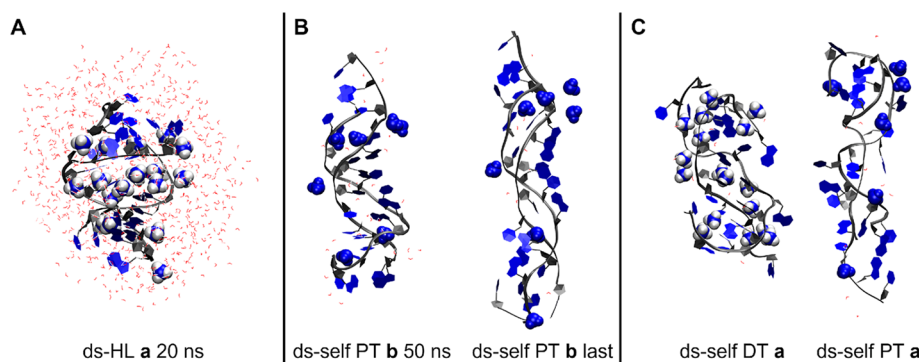


**Figure 8.** Snapshots of the MD simulation of the droplet evaporation: (A) ds-HL surrounded by water molecules (in red-white), with major groove zipping by ammonium ions. (B) structure modification of ds-self during the last part of the evaporation (PT stands for progressive proton transfer and 50 ns/last means the presented structures are obtained after 50 ns or at the end of the MD simulations) and (C) differences at the end of the simulation between the direct proton transfer (DT) and the progressive proton transfer (PT) for ds-self. (a and b) Full MD and a restart of the full MD after 10 ns, respectively. More details can be found in the methodology.

the experimental  ${}^{\text{DT}}\text{CCS}_{\text{He}}$  in Table 1. The CCS differ by 1 to 27% much less than the 18 to 35% range previously determined with the LC model, clearly confirming the key role played by the droplet evaporation process, and specifically the role of the ammonium ions, to generate more compact structures when the ds-DNA ions are transferred from the solution to the gas phase. Globally, ds-self affords more extended structures than ds-HL, which has a maximum overestimation of only 6%. Our MD simulations support that the broad experimental CCS distributions shown in Figure 2 result from a mixture of different ion conformations with different CCS. As an example, ds-HL PT a and ds-HL PT b present CCS at 792 and 790  $\text{\AA}^2$ , respectively, but possess slightly different structures as observed both on the snapshot and the HB heat map shown in Figure 9 (bottom). Furthermore, as shown in Figure S17, the CCS distributions derived from the MD simulations are too narrow compared to

**Table 1. Experimental and Theoretical CCS Obtained with the Different Droplet Evaporation Methods for ds-self and ds-HL 5– Ions<sup>a</sup>**

Structures	${}^{\text{TM}}\text{CCS}_{\text{He}}$ ( $\text{\AA}^2$ )	${}^{\text{DT}}\text{CCS}_{\text{He}}$ ( $\text{\AA}^2$ )	$\Delta\text{CCS}$ (%)
ds-HL DT a	761	751	1
ds-HL DT b	779		4
ds-HL PT a	792		6
ds-HL PT b	790		5
ds-self DT a	823	757	9
ds-self DT b	874		15
ds-self PT a	904		19
ds-self PT b	964		27

<sup>a</sup>a and b, respectively, identify the full MD simulation and a restart of the full MD after 10 ns. DT and PT, respectively, stand for at-the-end direct proton transfer and progressive proton transfer.

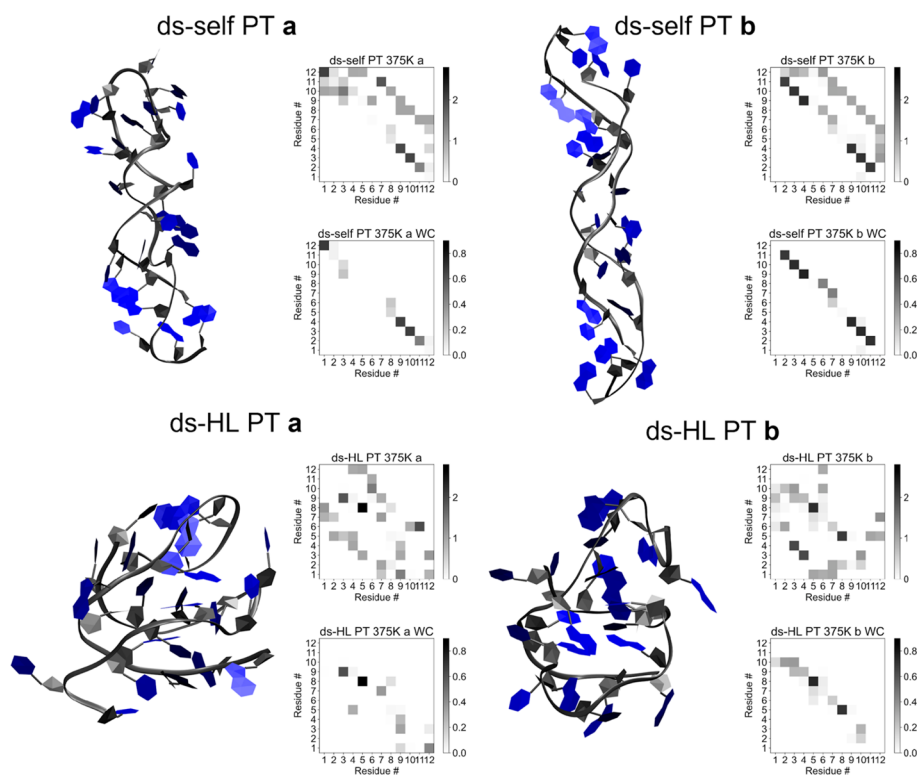


**Figure 9.** Snapshots of the last frame of the gas-phase MD following the droplet evaporation and the corresponding heat maps of HB for extended ds-self conformation (top) and compact ds-HL conformation (bottom). Top heat maps take all HB into account, while the bottom heat maps represent only the WC HB, after normalization. The top right diagonal corresponds to HB in the minor groove, while the bottom left diagonal corresponds to HB in the major groove.

the experimental ones. However, if we combine all the conformations obtained by the MD simulations of the droplet evaporation, they have structures and CCS that differ enough to produce a global CCS distribution as broad as the experimental one (Figure S17).

The most compact structure (ds-HL DT a) has a theoretical CCS at  $761 \text{ \AA}^2$ , really close to the apex of the experimental CCS distribution ( $757 \text{ \AA}^2$ , Figure 2). The compactness of this structure was analyzed based on its radial distribution function (RDF) calculated from its center of mass, as used in a previous study on dendrimer ions.<sup>25</sup> The RDF curve follows the typical trend of a compact globular structure with an initial parabolic increase of the atomic density, followed by a sharp decrease (see Figure S18). We believe that the  $^{\text{TM}}\text{CCS}_{\text{He}}$  are still probably overestimated, maybe due to the parametrization of the force field for solvent simulations, while it was here used for gas-phase investigation. In other words, small differences in interatomic distances can have a high impact when the number of atoms increases, e.g., the van der Waals equilibrium distance for H–H in the Dreiding force field leading to underestimated densities.<sup>48</sup> Another cause may come from the program used for the CCS calculation that also induces an overestimation of the CCS increasing with the size of the system.<sup>47</sup> Therefore, some of the structures outside of the experimental distribution could still be relevant.

As a general observation, the conformations obtained for ds-HL ions are more compact than those for ds-self ions. The CCS differences between the two sequences are probably due to the sampling rather than an effect of the sequences themselves, as the experimental CCS distributions are almost identical. As discussed above, a zipping caused by the ammonium ions occurs

for ds-HL early during the droplet evaporation, and remains until the end of the evaporation, leading to the most compact structures of all the sequences. A similar zipping process would give compact structures for ds-self as well, as obtained by Porrini et al.,<sup>28</sup> but was not observed during the time scale of our simulations. To afford compact structures with CCS around  $750 \text{ \AA}^2$  on the same sequence, Porrini et al.<sup>28</sup> forced the zipping, i.e., used constraints during the minimization to force the phosphates to form HB in both grooves.<sup>28</sup> This guided procedure allows to obtain quickly zipped structures but prevents the system from exploring all the other relevant conformations.

HB heat maps for selected compact and extended structures are presented in Figure 9. Extended structures, such as ds-self PT a and b, are characterized by two diagonals, i.e., the WC and the minor groove zipping diagonals, reminiscent to the HB heat maps generated for the extended structures obtained with the LC method (Figure S10). The extended conformations conserve the WC HB to a larger extent than the compact ones, with well-defined WC diagonals (except for the weaker AT interactions). On the other hand, the most compact conformations, i.e., ds-HL (Figure 9), systematically possess the diagonal corresponding to the major groove zipping, but not always the one corresponding to the minor groove zipping. The other structures and HB heat maps can be found in Figures S19–22.

*Molecular Dynamics Simulations on Gaseous Dendriplex 5–Ions.* At the beginning of the previous section, we wrote that the direct formation of gas phase ds-DNA ions via the LC (localized charge) model systematically generates extended structures not representative of the experimental data, since the

zipping role of the ammonium ion is not considered. For dendriplex ions, the dendrimer partners are protonated and are thus likely to fulfill the role of the ammonium ions during the solvent molecule evaporation. Therefore, we decided to first test whether the LC model protocol may reproduce the experimental structures of gaseous dendriplex ions. The point here is to determine whether the complexation can prevent the extension of the structure during an abrupt transition from solution to gas phase in MD simulations, without considering the progressive solvent molecule evaporation.

When involved in the neutralization of ds-DNA ions upon ESI, ammonium cations ( $\text{NH}_4^+$ ) transfer their protons to the proximal phosphate groups before being expelled as neutral ammonia. For the dendriplex ions, we first demonstrated based on proton affinity (PA) calculations (see [Methodology](#)) that 5–dendriplex ions are best described as the combination between a neutral dendrimer and a 5– ds-DNA, instead of an association between a fully protonated 4+ dendrimer and a 9– ds-DNA. The main difference with respect to the ds-DNA ionization is that the dendrimer remains attached on the ds-DNA at the end of the ESI process, whereas ammonia molecules are evaporated.

The dendriplex ion input structures were then prepared from the five most stable dendriplex structures generated in solution (see previous section). The dendrimers were then made neutral by removing the protons at the four ammonium end groups, and the phosphate groups of ds-DNA were protonated to localize the charges on the same residues as for ds-DNA alone to reach 5–ions. Two charge locations **A** and **B** were considered due to the asymmetric distribution of five negative charges on two DNA strands leading to ten gas phase structures for each dendriplex ions. Then MD simulations were performed and CCS extracted. Experimental ( $^{DT}\text{CCS}_{\text{He}}$ ) and theoretical ( $^{\text{TM}}\text{CCS}_{\text{He}}$ ) values are listed in [Tables S3–4](#). We previously showed that the LC model afforded theoretical DNA CCS overestimated by at least 18% when compared to the experimental ones. Overestimations between 4 and 37% for the dendriplex ions are obtained, revealing that compact structures may be produced for dendriplex ions, even with the LC model. This result demonstrates that the dendrimer contributes to the compaction of the DNA structure, somehow preventing the ion from unfolding. From [Tables S3–4](#), we observe that the final structure in the gas phase depends more on the initial dendrimer position than on the position of the charges (**A** or **B**).

In [Figures S24–31](#), the gas-phase structures are gathered with the corresponding HB heat maps. The analysis of the HB heat maps is less straightforward than for ds-DNA due to the additional presence of the DNA/dendrimer interactions. As typical examples, [Figure 10](#) presents structures generated for the association between ds-self and E0 considering the **A** and **B** negative charge distributions. When comparing ds-self E0 20 **A** and **B**, we first observe the conservation of the WC base pairing and that the two different charge locations (**A** vs **B**) afford similar final structures and HB heat maps. However, for some specific cases, as ds-self E0 7 **A** and **B**, significantly different conformations are generated. As for ds-DNA described in the previous section, the extended conformations are characterized by HB between phosphate groups in the minor groove, highlighted by the top-right offset diagonal in the heat maps, see ds-self E0 20 **A** as a typical case. Regarding the compact conformations, which are more experimentally relevant than the extended ones, the structures also present some phosphate-phosphate HB in the bottom-left part, as seen for ds-HL P1 42 **A**

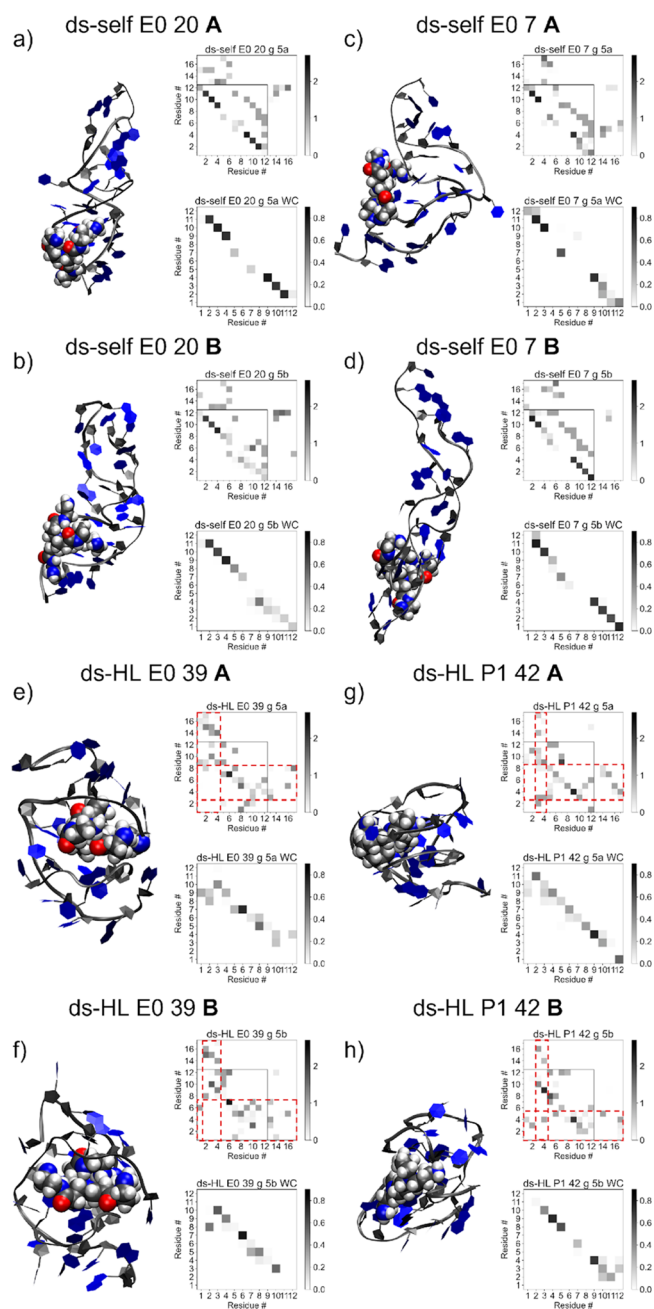


**Figure 10.** Last frames of the gas phase MD (LC) for dendriplex 5–ions associating ds-self and E0 (a–d), ds-HL and E0 (e–f), and ds-HL and P1 (g–h) and the corresponding HB heat maps to highlight the influence of the asymmetric charge location. For each structure, the top heat map takes all HB into account, while the bottom heat map represents only the WC HB, after normalization. The DNA backbone is in gray and the nucleobases are in blue. The dendrimer is represented as vdw spheres with colors representing the atoms: carbon (gray), hydrogen (white), oxygen (red), and nitrogen (blue). The numbers correspond to the input numbers.

and **B** in [Figure 10](#), corresponding to interactions in the major groove, though both zippings are incomplete.

The global HB heat maps can also be used to detect the dendrimer/DNA interaction site, and the compact conformations, such as ds-HL E0 39 **A** and ds-HL P1 42 **B** ([Figure 10](#)), present interactions in the major groove. This interaction brings the two strands together, compacting the DNA conformation. We thus found here that the compaction by the dendrimer is

mainly due to major groove bridging. The compaction of the conformation is thus associated with HB between phosphates (groove zipping) and HB interactions between dendrimer moieties and DNA (groove bridging). Overall, the conformational heterogeneity should be responsible for the broad experimental CCS distributions of Figure 2.

In addition to the LC model, droplets containing dendriplexes were also created and progressively evaporated to investigate the role both of a progressive transfer from solution to gas phase and of the additional ammonium ions on the dendriplex gas phase structures. Indeed, the global charge of the droplet being 5<sup>-</sup>, and considering that the ds-DNA and the dendrimers carry 22<sup>-</sup> and 4<sup>+</sup> charges, respectively, 13 NH<sub>4</sub><sup>+</sup> ions were added in the droplet. The droplets were created only for the most stable solution structure (Table S1 and Figures S1,3,5,7). Hence, the dendrimer being initially positively charged, the proton transfer from the dendrimer ammonium groups to the phosphate groups was performed using the progressive proton transfer protocol (PT) or the direct proton transfer protocol (DT), as used previously for ds-DNA ions. For the dendriplexes, as for the DNA duplexes previously studied, two MD simulations were performed. Snapshots of the evaporation process are presented in Figures S32–39. Contrary to ds-DNA ions, the conformations of the dendriplex ions did not expand during the evaporation of the droplet but shrank compared to the starting structure (Figure 11).

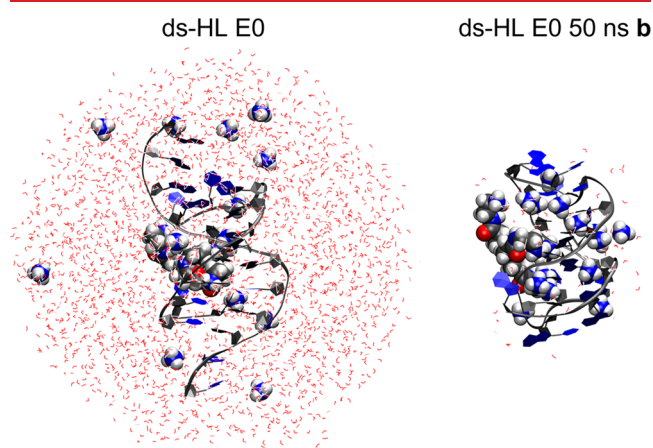


**Figure 11.** Snapshots from the droplet evaporation showing the structure shrinkage of ds-HL E0 dendriplex 5<sup>-</sup> ions upon evaporation.

Once desolvated and protonated, the ions were submitted to gas phase MD. The <sup>TM</sup>CCS<sub>He</sub> values obtained for those ions are gathered in Table S5 along with the experimental <sup>DT</sup>CCS<sub>He</sub>. With the droplet evaporation method, the CCS differences are between 1 and 18%, compared to 4 to 37% for the LC model, demonstrating that the droplet evaporation induces a structural compaction for the dendriplexes, as it was also observed for ds-DNA in the present study and in the literature.<sup>28</sup>

The final gas-phase structures and the related HB heat maps are represented in Figures S40–47. For ds-DNA alone, we observed that both the WC diagonal and the minor groove zipping (top-right diagonal) characterize the extended structures and that the compact structures present both minor groove zipping and major groove zipping (bottom-left diagonal). For the dendriplexes, we observed that clear WC and minor groove zipping still correspond to extended conformations, although

less extended than for ds-DNA alone (ds-HL E0 PT a, ds-self P1 b, and PT a in Figure 12).

For compact structures, the partial minor or major groove zipping by HB between phosphate groups is completed by DNA/dendrimer interactions in the major groove (ds-self E0 PT a, ds-self P1 a, and ds-HL PT b in Figure 12), resulting in major groove bridging. These results show the same tendencies as those obtained with the LC model, but with an improved groove zipping and bridging, which likely explains the additional compaction of the structure when using the droplet evaporation protocol.

## CONCLUSIONS

In this paper, we combined IMS experiments and MD modeling to obtain structural information on gas-phase dendriplex ions. As these systems can undergo conformational changes when transferred from solution to the gas phase in MS experiments, due to the loss of water, protonation, and the evolution of the net charge (from 22<sup>-</sup> in solution to 5<sup>-</sup> in the gas phase), we evaluated the impact of the solution to gas-phase transfer on the dendriplex conformation.

We first studied DNA duplexes. We confirmed that the direct formation of the ions in the gas phase from the solution structure results in too extended structures compared to the experiments. Coulomb repulsion between negatively charged phosphates prevents phosphates from getting close enough to bind by HB and compact the structure. To obtain structures as compact as the experimental ones, we had to simulate the transfer of the ions from solution to gas phase, i.e., via the formation of droplets followed by their evaporation. Droplet evaporation allows a reorganization and compaction of the structure mediated by the ammonium ions, which interact with the phosphates in both DNA grooves, bring the strands close enough to allow groove zipping by HB after transferring a proton to phosphates, then evaporate as ammonia.

The comparison of the simulated and experimental CCS distributions showed that different structures coexist, as the experimental CCS distribution is much wider than the simulated distribution. Thus, the experimental width reflects a distribution of conformation, resulting from a distribution of protonation pathways driving the conformational rearrangement upon desolvation. Several candidate conformations found by MD simulations have partially conserved the Watson–Crick HB pattern, and do not interconvert in the time scale of the dynamics (200 ns), which is small compared to the experimental time scale (1–10 ms). Two methods were used to simulate the droplet evaporation: one where the proton transfer from ammonium to phosphates occurs along the evaporation, and one where the transfer occurs at once at the end of the evaporation. Both approaches give conformations with a similar range of CCS values, suggesting that the kinetics of proton relocation from ammonium to phosphates is not critical for the structure compactness. However, the statistics is not large enough to give definite conclusions. For the dendriplex ions, the DNA sequence has no impact on the CCS distributions.

MD simulations showed that several dendriplex conformations coexist in solution, with the dendrimer interacting either in the major groove or in the minor groove of DNA. The Watson–Crick HB pattern is well-preserved. Once in the gas phase, these structures contract, and their Watson–Crick HB pattern is only partly conserved. Unlike for ds-DNA, we could directly simulate compact structures via the LC method thanks to interactions between DNA phosphate groups and the dendrimers terminal

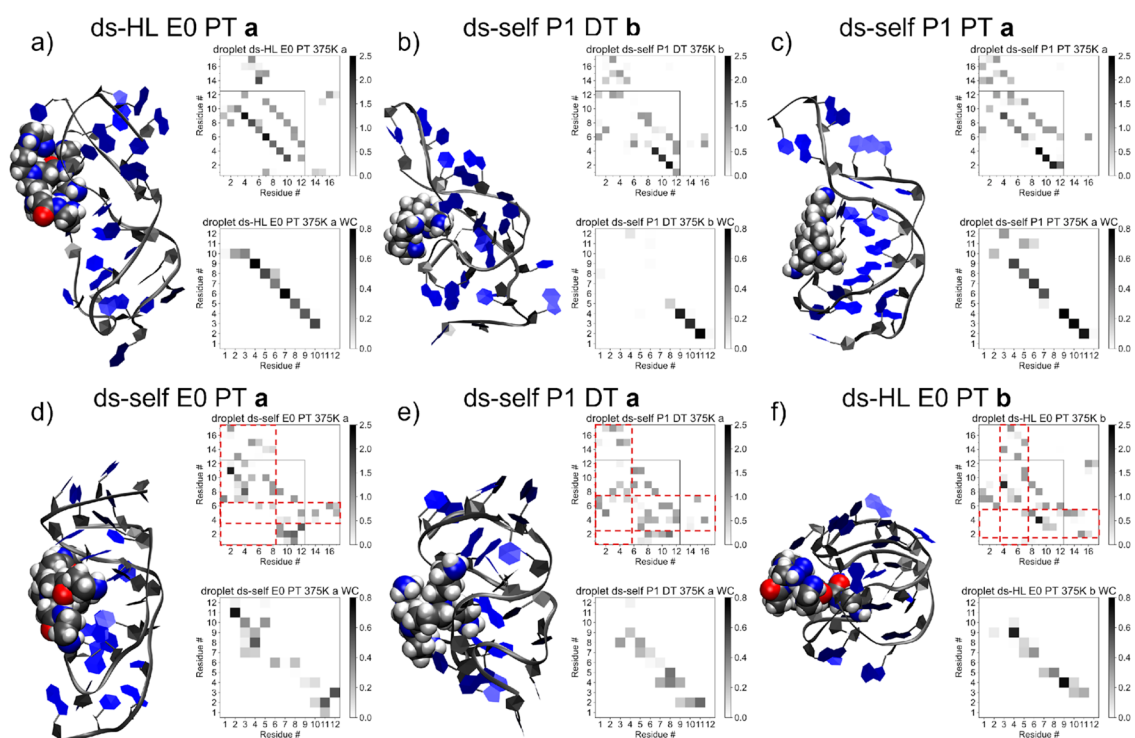


**Figure 12.** Snapshots of the last frame of the gas phase MD following the droplet evaporation and the corresponding heat maps of HB for extended dendriplex 5<sup>-</sup> ion conformations with minor groove diagonal (a–c) and compact conformations (d–f). For each structure, the top heat map takes all HB into account, while the bottom heat map represents only the WC HB.

protonated amines, but the droplet evaporation protocol gives even more compact structures through additional ammonium-phosphate interactions. Ammonium cations and dendrimer protonated amines help bridging both major and minor grooves, leading to structural compaction. After the proton transfer, ammonia evaporates, but the grooves are maintained contracted by zipping thanks to HB between phosphates (as the neutralization adds a proton). In other groove locations, some bridges are maintained via the neutralized terminal amines of the dendrimer.

As ion mobility mass spectrometry together with molecular dynamics simulations is increasingly used to study biomolecules, such as proteins and nucleic acids, due to the intrinsic properties of mass spectrometry (sensitivity, selectivity and rapidity), we believe that our contribution represents a step further in the understanding of the ionization mechanisms of DNA and DNA complexes. Also, this contribution again demonstrates that force field Molecular Dynamics simulations must be handled with great care by explicitly considering the physicochemical processes undergone by the ions from the solution to the gas phase.

## ■ ASSOCIATED CONTENT

### SI Supporting Information

The Supporting Information is available free of charge at <https://pubs.acs.org/doi/10.1021/jasms.2c00122>.

(Table S1) Solution Molecular Dynamics data (energies) for stable dendriplexes; (Tables S2–5) Experimental and theoretical CCS for the duplex 5<sup>-</sup> ions (LC model), for the dendriplex 5<sup>-</sup> ions (E0-LC model), for the dendriplex 5<sup>-</sup> ions (P1-LC model), and for the three dendriplex ions produced upon droplet evaporation simulation; Figures S1,3,5,7,9,10,13–16,19,21,23,24,26,28,30,32–39,-

40,42,44,46 present the structures obtained using MD simulations for the duplex and dendriplex ions; Figures S2,4,6,11,20,22,25,27,29,31,41,43,45,47 present the hydrogen bond heat maps for the duplex and dendriplex ions; Figure S12 presents the evolution of the water molecule evaporation all along the MD simulation from ds-self-droplet; Figure S17 presents the comparison between theoretical CCS distributions and experimental data, and Figure S18 features the radial distribution functions (RDF) for selected 5<sup>-</sup> dendriplex ions (PDF)

## ■ AUTHOR INFORMATION

### Corresponding Author

Pascal Gerbaux – Organic Synthesis & Mass Spectrometry Laboratory, Interdisciplinary Center for Mass Spectrometry (CISMa), Center of Innovation and Research in Materials and Polymers (CIRMAP), University of Mons - UMONS, 7000 Mons, Belgium; [orcid.org/0000-0001-5114-4352](https://orcid.org/0000-0001-5114-4352); Email: [pascal.gerbaux@umons.ac.be](mailto:pascal.gerbaux@umons.ac.be)

### Authors

Fabrice Saintmont – Organic Synthesis & Mass Spectrometry Laboratory, Interdisciplinary Center for Mass Spectrometry (CISMa), Center of Innovation and Research in Materials and Polymers (CIRMAP) and Laboratory for Chemistry of Novel Materials, Center of Innovation and Research in Materials and Polymers, Research Institute for Science and Engineering of Materials, University of Mons - UMONS, 7000 Mons, Belgium  
Sébastien Hoyas – Organic Synthesis & Mass Spectrometry Laboratory, Interdisciplinary Center for Mass Spectrometry (CISMa), Center of Innovation and Research in Materials and Polymers (CIRMAP) and Laboratory for Chemistry of Novel Materials, Center of Innovation and Research in Materials and

Polymers, Research Institute for Science and Engineering of Materials, University of Mons - UMONS, 7000 Mons, Belgium  
Frédéric Rosu – Univ. Bordeaux, CNRS, INSERM, Institut Européen de Chimie et Biologie (IECB, UAR3033, US001), 33607 Pessac, France; [orcid.org/0000-0003-3674-7539](https://orcid.org/0000-0003-3674-7539)

Valérie Gabelica – Univ. Bordeaux, CNRS, INSERM, Institut Européen de Chimie et Biologie (IECB, UAR3033, US001), 33607 Pessac, France; Univ. Bordeaux, INSERM, CNRS, Acides Nucléiques Régulations Naturelle et Artificielle (ARNA, U1212, UMR5320), IECB, 33607 Pessac, France; [orcid.org/0000-0001-9496-0165](https://orcid.org/0000-0001-9496-0165)

Patrick Brocorens – Laboratory for Chemistry of Novel Materials, Center of Innovation and Research in Materials and Polymers, Research Institute for Science and Engineering of Materials, University of Mons - UMONS, 7000 Mons, Belgium

Complete contact information is available at:  
<https://pubs.acs.org/10.1021/jasms.2c00122>

## Notes

The authors declare no competing financial interest.

## ACKNOWLEDGMENTS

The drift tube IMS experiments were carried out at the Plateforme de BioPhysicochimie Structurale of the IECB. F.S. and S.H. thank the University of Mons and the “Fonds pour la Recherche Industrielle et Agricole” for their Ph.D. grants. The work in the Laboratory for Chemistry of Novel Materials was supported by the “Consortium des Equipements de Calcul Intensif” funded by the Fonds National de la Recherche Scientifique (F.R.S.-FNRS) under Grant No. 2.5020.11.

## REFERENCES

- (1) Dufès, C.; Uchegbu, I. F.; Schätzlein, A. G. Dendrimers in Gene Delivery. *Adv. Drug Delivery Rev.* **2005**, *57* (15), 2177–2202.
- (2) Pack, D. W.; Hoffman, A. S.; Pun, S.; Stayton, P. S. Design and Development of Polymers for Gene Delivery. *Nat. Rev. Drug Discovery* **2005**, *4* (7), 581–593.
- (3) van den Berg, A. I. S.; Yun, C.-O.; Schifflers, R. M.; Hennink, W. E. Polymeric Delivery Systems for Nucleic Acid Therapeutics: Approaching the Clinic. *J. Controlled Release* **2021**, *331*, 121–141.
- (4) Luo, D.; Saltzman, W. M. Synthetic DNA Delivery Systems. *Nat. Biotechnol.* **2000**, *18* (1), 33–37.
- (5) Mintzer, M. A.; Simanek, E. E. Nonviral Vectors for Gene Delivery. *Chem. Rev.* **2009**, *109* (2), 259–302.
- (6) Haensler, J.; Szoka, F. C. Polyamidoamine Cascade Polymers Mediate Efficient Transfection of Cells in Culture. *Bioconjugate Chem.* **1993**, *4* (5), 372–379.
- (7) Kukowska-Latallo, J. F.; Bielinska, A. U.; Johnson, J.; Spindler, R.; Tomalia, D. A.; Baker, J. R. Efficient Transfer of Genetic Material into Mammalian Cells Using Starburst Polyamidoamine Dendrimers. *Proc. Natl. Acad. Sci. U. S. A.* **1996**, *93* (10), 4897–4902.
- (8) Navarro, G.; Tros de Ilarduya, C. Activated and Non-Activated PAMAM Dendrimers for Gene Delivery in Vitro and in Vivo. *Nanomedicine. NBM* **2009**, *5* (3), 287–297.
- (9) Alajangi, H. K.; Natarajan, P.; Vij, M.; Ganguli, M.; Santhiya, D. Role of Unmodified Low Generation – PAMAM Dendrimers in Efficient Non-Toxic Gene Transfection. *ChemistrySelect* **2016**, *1* (16), 5206–5217.
- (10) Shcharbin, D.; Pedziwiatr, E.; Bryszewska, M. How to Study Dendriplexes I: Characterization. *J. Controlled Release* **2009**, *135* (3), 186–197.
- (11) Shen, X.-C.; Zhou, J.; Liu, X.; Wu, J.; Qu, F.; Zhang, Z.-L.; Pang, D.-W.; Quéléver, G.; Zhang, C.-C.; Peng, L. Importance of Size-to-Charge Ratio in Construction of Stable and Uniform Nanoscale RNA/Dendrimer Complexes. *Org. Biomol. Chem.* **2007**, *5* (22), 3674.
- (12) Braun, C. S.; Vetro, J. A.; Tomalia, D. A.; Koe, G. S.; Koe, J. G.; Russell Middaugh, C. Structure/Function Relationships of Polyamidoamine/DNA Dendrimers as Gene Delivery Vehicles. *J. Pharm. Sci.* **2005**, *94* (2), 423–436.
- (13) Jensen, L. B.; Pavan, G. M.; Kasimova, M. R.; Rutherford, S.; Danani, A.; Nielsen, H. M.; Foged, C. Elucidating the Molecular Mechanism of PAMAM-SiRNA Dendriplex Self-Assembly: Effect of Dendrimer Charge Density. *Int. J. Pharm.* **2011**, *416* (2), 410–418.
- (14) Alajangi, H. K.; Santhiya, D. Fluorescence and Förster Resonance Energy Transfer Investigations on DNA Oligonucleotide and PAMAM Dendrimer Packing Interactions in Dendriplexes. *Phys. Chem. Chem. Phys.* **2015**, *17* (14), 8680–8691.
- (15) Jain, A.; Mahira, S.; Majoral, J. P.; Bryszewska, M.; Khan, W.; Ionov, M. Dendrimer Mediated Targeting of SiRNA against Polo-like Kinase for the Treatment of Triple Negative Breast Cancer. *J. Biomed. Mater. Res. - Part A* **2019**, *107* (9), 1933–1944.
- (16) Maiti, P. K.; Bagchi, B. Structure and Dynamics of DNA–Dendrimer Complexation: Role of Counterions, Water, and Base Pair Sequence. *Nano Lett.* **2006**, *6* (11), 2478–2485.
- (17) Vasumathi, V.; Maiti, P. K. Complexation of SiRNA with Dendrimer: A Molecular Modeling Approach. *Macromolecules* **2010**, *43* (19), 8264–8274.
- (18) Nandy, B.; Maiti, P. K. DNA Compaction by a Dendrimer. *J. Phys. Chem. B* **2011**, *115* (2), 217–230.
- (19) Lary, E.; König, A.; Ghosh, A.; Ghosh, D.; Benabou, S.; Rosu, F.; Gabelica, V. Mass Spectrometry of Nucleic Acid Noncovalent Complexes. *Chem. Rev.* **2022**, *122* (8), 7720–7839.
- (20) Leriche, E. D.; Hubert-Roux, M.; Afonso, C.; Lange, C. M.; Grosse, M. C.; Maire, F.; Loutelier-Bourhis, C. Investigation of Dendriplexes by Ion Mobility-Mass Spectrometry. *Molecules* **2014**, *19* (12), 20731–20750.
- (21) D’Atri, V.; Porrini, M.; Rosu, F.; Gabelica, V. Linking Molecular Models with Ion Mobility Experiments. Illustration with a Rigid Nucleic Acid Structure. *J. Mass Spectrom.* **2015**, *50* (5), 711–726.
- (22) Mao, Y.; Woenckhaus, J.; Kolafa, J.; Ratner, M. A.; Jarrold, M. F. Thermal Unfolding of Unsolvated Cytochrome c: Experiment and Molecular Dynamics Simulations. *J. Am. Chem. Soc.* **1999**, *121* (12), 2712–2721.
- (23) Lanucara, F.; Holman, S. W.; Gray, C. J.; Evers, C. E. The Power of Ion Mobility-Mass Spectrometry for Structural Characterization and the Study of Conformational Dynamics. *Nat. Chem.* **2014**, *6* (4), 281–294.
- (24) Duez, Q.; Hoyas, S.; Josse, T.; Cornil, J.; Gerbaux, P.; De Winter, J. Gas-phase Structure of Polymer Ions: Tying Together Theoretical Approaches and Ion Mobility Spectrometry. *Mass Spectrom. Rev.* **2021**, DOI: 10.1002/mas.21745.
- (25) Saintmont, F.; De Winter, J.; Chiro, F.; Halin, E.; Dugourd, P.; Brocorens, P.; Gerbaux, P. How Spherical Are Gaseous Low Charged Dendrimer Ions: A Molecular Dynamics/Ion Mobility Study? *J. Am. Soc. Mass Spectrom.* **2020**, *31* (8), 1673–1683.
- (26) Tintaru, A.; Pricl, S.; Denbigh, L.; Liu, X.; Peng, L.; Charles, L. Conformational Changes of Small PAMAM Dendrimers as a Function of Their Charge State: A Combined Electrospray Mass Spectrometry, Traveling-Wave Ion Mobility and Molecular Modeling Study. *Int. J. Mass Spectrom.* **2013**, *354–355*, 235–241.
- (27) Abi-Ghanem, J.; Gabelica, V. Nucleic Acid Ion Structures in the Gas Phase. *Phys. Chem. Chem. Phys.* **2014**, *16* (39), 21204–21218.
- (28) Porrini, M.; Rosu, F.; Rabin, C.; Darré, L.; Gómez, H.; Orozco, M.; Gabelica, V. Compaction of Duplex Nucleic Acids upon Native Electrospray Mass Spectrometry. *ACS Cent. Sci.* **2017**, *3* (5), 454–461.
- (29) Lipfert, J.; Doniach, S.; Das, R.; Herschlag, D. Understanding Nucleic Acid–Ion Interactions. *Annu. Rev. Biochem.* **2014**, *83* (1), 813–841.
- (30) Gabelica, V.; Shvartsburg, A. A.; Afonso, C.; Barran, P.; Benesch, J. L. P.; Bleiholder, C.; Bowers, M. T.; Bilbao, A.; Bush, M. F.; Campbell, J. L.; Campuzano, I. D. G.; Causon, T.; Clowers, B. H.; Creaser, C. S.; De Pauw, E.; Far, J.; Fernandez-Lima, F.; Fjeldsted, J. C.; Giles, K.; Groessl, M.; Hogan, C. J.; Hann, S.; Kim, H. I.; Kurulugama, R. T.; May, J. C.; McLean, J. A.; Pagel, K.; Richardson, K.; Ridgeway, M.

E.; Rosu, F.; Sobott, F.; Thalassinou, K.; Valentine, S. J.; Wyttenbach, T. Recommendations for Reporting Ion Mobility Mass Spectrometry Measurements. *Mass Spectrom. Rev.* **2019**, *38* (3), 291–320.

(31) Gabelica, V.; Livet, S.; Rosu, F. Optimizing Native Ion Mobility Q-TOF in Helium and Nitrogen for Very Fragile Noncovalent Structures. *J. Am. Soc. Mass Spectrom.* **2018**, *29* (11), 2189–2198.

(32) Marchand, A.; Livet, S.; Rosu, F.; Gabelica, V. Drift Tube Ion Mobility: How to Reconstruct Collision Cross Section Distributions from Arrival Time Distributions? *Anal. Chem.* **2017**, *89* (23), 12674–12681.

(33) Maingi, V.; Jain, V.; Bharatam, P. V.; Maiti, P. K. Dendrimer Building Toolkit: Model Building and Characterization of Various Dendrimer Architectures. *J. Comput. Chem.* **2012**, *33* (25), 1997–2011.

(34) Ivani, I.; Dans, P. D.; Noy, A.; Pérez, A.; Faustino, I.; Hospital, A.; Walther, J.; Andrio, P.; Goñi, R.; Balaceanu, A.; Portella, G.; Battistini, F.; Gelpí, J. L.; González, C.; Vendruscolo, M.; Laughton, C. A.; Harris, S. A.; Case, D. A.; Orozco, M. Parmbsc1: A Refined Force Field for DNA Simulations. *Nat. Methods* **2016**, *13* (1), 55–58.

(35) Wang, J.; Wolf, R. M.; Caldwell, J. W.; Kollman, P. A.; Case, D. A. Development and Testing of a General Amber Force Field. *J. Comput. Chem.* **2004**, *25* (9), 1157–1174.

(36) Case, D. A.; Betz, R. M.; Cerutti, D. S.; Cheatham, III, T. E.; Darden, T. A.; Duke, R. E.; Giese, T. J.; Gohlke, H.; Goetz, A. W.; Homeyer, N.; Izadi, S.; Janowski, P.; Kaus, J.; Kovalenko, A.; Lee, T. S.; LeGrand, S.; Li, P.; Lin, C.; Luchko, T.; Luo, R.; Madej, B.; Mermelstein, D.; Merz, K. M.; Monard, G.; Nguyen, H.; Nguyen, H. T.; Omelyan, I.; Onufriev, A.; Roe, D. R.; Roitberg, A.; Sagui, C.; Simmerling, C. L.; Botello-Smith, W. M.; Swails, J.; Walker, R. C.; Wang, J.; Wolf, R. M.; Wu, X.; Xiao, L.; Kollman, P. A. *Amber 2016*; University of California, San Francisco. 2016.

(37) Hawkins, G. D.; Cramer, C. J.; Truhlar, D. G. Pairwise Solute Descreening of Solute Charges from a Dielectric Medium. *Chem. Phys. Lett.* **1995**, *246* (1–2), 122–129.

(38) Frisch, M. J.; Trucks, G. W.; Schlegel, H. B.; Scuseria, G. E.; Robb, M. A.; Cheeseman, J. R.; Scalmani, G.; Barone, V.; Petersson, G. A.; Nakatsuji, H.; Li, X.; Caricato, M.; Marenich, A. V.; Bloino, J.; Janesko, B. G.; Gomperts, R.; Mennucci, B.; Hratchian, H. P.; Ortiz, J. V.; Izmaylov, A. F.; Sonnenberg, J. L.; Williams-Young, D.; Ding, F.; Lipparini, F.; Egidi, F.; Goings, J.; Peng, B.; Petrone, A.; Henderson, T.; Ranasinghe, D.; Zakrzewski, V. G.; Gao, J.; Rega, N.; Zheng, G.; Liang, W.; Hada, M.; Ehara, M.; Toyota, K.; Fukuda, R.; Hasegawa, J.; Ishida, M.; Nakajima, T.; Honda, Y.; Kitao, O.; Nakai, H.; Vreven, T.; Throssell, K.; Montgomery, J. A., Jr.; Peralta, J. E.; Ogliaro, F.; Bearpark, M. J.; Heyd, J. J.; Brothers, E. N.; Kudin, K. N.; Staroverov, V. N.; Keith, T. A.; Kobayashi, R.; Normand, J.; Raghavachari, K.; Rendell, A. P.; Burant, J. C.; Iyengar, S. S.; Tomasi, J.; Cossi, M.; Millam, J. M.; Klene, M.; Adamo, C.; Cammi, R.; Ochterski, J. W.; Martin, R. L.; Morokuma, K.; Farkas, O.; Foresman, J. B.; Fox, D. J. *Gaussian 16*; Gaussian, Inc., 2016.

(39) Jorgensen, W. L.; Chandrasekhar, J.; Madura, J. D.; Impey, R. W.; Klein, M. L. Comparison of Simple Potential Functions for Simulating Liquid Water. *J. Chem. Phys.* **1983**, *79* (2), 926–935.

(40) Martínez, L.; Andrade, R.; Birgin, E. G.; Martínez, J. M. PACKMOL: A Package for Building Initial Configurations for Molecular Dynamics Simulations. *J. Comput. Chem.* **2009**, *30* (13), 2157–2164.

(41) McAllister, R. G.; Metwally, H.; Sun, Y.; Konermann, L. Release of Native-like Gaseous Proteins from Electrospray Droplets via the Charged Residue Mechanism: Insights from Molecular Dynamics Simulations. *J. Am. Chem. Soc.* **2015**, *137* (39), 12667–12676.

(42) Konermann, L.; Aliyari, E.; Lee, J. H. Mobile Protons Limit the Stability of Salt Bridges in the Gas Phase: Implications for the Structures of Electrosprayed Protein Ions. *J. Phys. Chem. B* **2021**, *125* (15), 3803–3814.

(43) Marchese, R.; Grandori, R.; Carloni, P.; Raugei, S. A Computational Model for Protein Ionization by Electrospray Based on Gas-Phase Basicity. *J. Am. Soc. Mass Spectrom.* **2012**, *23* (11), 1903–1910.

(44) Li, J.; Lyu, W.; Rossetti, G.; Konijnenberg, A.; Natalello, A.; Ippoliti, E.; Orozco, M.; Sobott, F.; Grandori, R.; Carloni, P. Proton Dynamics in Protein Mass Spectrometry. *J. Phys. Chem. Lett.* **2017**, *8* (6), 1105–1112.

(45) Konermann, L.; Kim, S. Grotthuss Molecular Dynamics Simulations for Modeling Proton Hopping in Electrosprayed Water Droplets. *J. Chem. Theory Comput.* **2022**, *18*, 3781.

(46) Roe, D. R.; Cheatham, T. E. PTRAJ and CPPTRAJ: Software for Processing and Analysis of Molecular Dynamics Trajectory Data. *J. Chem. Theory Comput.* **2013**, *9* (7), 3084–3095.

(47) Ewing, S. A.; Donor, M. T.; Wilson, J. W.; Prell, J. S. Collidoscope: An Improved Tool for Computing Collisional Cross-Sections with the Trajectory Method. *J. Am. Soc. Mass Spectrom.* **2017**, *28* (4), 587–596.

(48) Sun, L.; Yang, L.; Zhang, Y. D.; Shi, Q.; Lu, R. F.; Deng, W. Q. Accurate van Der Waals Force Field for Gas Adsorption in Porous Materials. *J. Comput. Chem.* **2017**, *38* (23), 1991–1999.

## Recommended by ACS

### Influence of 5-Methylation and the 2'- and 3'-Hydroxy Substituents on the Base Pairing Energies of Protonated Cytidine Nucleoside Analogue Base Pairs: Implicatio...

Yakubu S. Seidu, M. T. Rodgers, *et al.*

JULY 06, 2021

THE JOURNAL OF PHYSICAL CHEMISTRY A

READ 

### Comprehensive Bioanalysis of Ultrahigh Molecular Weight, Highly Disperse Poly(ethylene oxide) in Rat via Microsolid Phase Extraction and RPLC-Q-Q-TOF Cou...

Zhi Zhang, Jingkai Gu, *et al.*

MARCH 26, 2020

ANALYTICAL CHEMISTRY

READ 

### HIV Reverse Transcriptase Pre-Steady-State Kinetic Analysis of Chain Terminators and Translocation Inhibitors Reveals Interactions between Magnesium...

Christopher R. Dilmore and Jeffrey J. DeStefano

MAY 25, 2021

ACS OMEGA

READ 

### Exploring the Conformational and Binding Dynamics of HMGA2-DNA Complexes Using Trapped Ion Mobility Spectrometry–Mass Spectrometry

Kevin Jeanne Dit Fouque, Francisco Fernandez-Lima, *et al.*

JUNE 10, 2022

JOURNAL OF THE AMERICAN SOCIETY FOR MASS SPECTROMETRY

READ 

Get More Suggestions >